

Review

# A Review on Recent Advances in Piezoelectric Ceramic 3D Printing

Jiwon Park <sup>1,†</sup> , Dong-Gyu Lee <sup>1,2,†</sup> , Sunghoon Hur <sup>1</sup> , Jeong Min Baik <sup>1,3,4</sup>, Hyun Soo Kim <sup>1,\*</sup> and Hyun-Cheol Song <sup>1,3,4,\*</sup> 

- <sup>1</sup> Electronic Materials Research Center, Korea Institute of Science and Technology (KIST), Seoul 02792, Republic of Korea  
<sup>2</sup> Materials Science and Engineering, Korea University, Seoul 02841, Republic of Korea  
<sup>3</sup> School of Advanced Materials Science and Engineering, Sungkyunkwan University (SKKU), Suwon 16419, Republic of Korea  
<sup>4</sup> KIST-SKKU Graphene-Neutral Research Center, Sungkyunkwan University (SKKU), Suwon 16419, Republic of Korea  
\* Correspondence: star92123@kist.re.kr (H.S.K.); hcsong@kist.re.kr (H.-C.S.)  
† These authors contributed equally to this work.

**Abstract:** Piezoelectric materials are a class of materials that can generate an electric charge when subjected to mechanical stress, or vice versa. These materials have a wide range of applications, from sensors and actuators to energy-harvesting devices and medical implants. Recently, there has been growing interest in using 3D printing to fabricate piezoelectric materials with complex geometries and tailored properties. Three-dimensional printing allows for the precise control of the material's composition, microstructure, and shape, which can significantly enhance piezoelectric materials' performance. Three-dimensional printing has emerged as a promising technique for fabricating piezoelectric materials with tailored properties and complex geometries. The development of high-performance piezoelectric materials using 3D printing could have significant implications for various applications, including sensors, energy harvesting, and medical devices. In this review paper, 3D printing methods for piezoelectric materials, their advantages and disadvantages, representative piezoelectric ceramics, and examples of 3D printing are presented. Furthermore, the applications utilizing these materials are summarized.



**Citation:** Park, J.; Lee, D.-G.; Hur, S.; Baik, J.M.; Kim, H.S.; Song, H.-C.

A Review on Recent Advances in Piezoelectric Ceramic 3D Printing. *Actuators* **2023**, *12*, 177. <https://doi.org/10.3390/act12040177>

Academic Editor: Junhui Hu

Received: 27 February 2023

Revised: 22 March 2023

Accepted: 23 March 2023

Published: 18 April 2023



**Copyright:** © 2023 by the authors. Licensee MDPI, Basel, Switzerland. This article is an open access article distributed under the terms and conditions of the Creative Commons Attribution (CC BY) license (<https://creativecommons.org/licenses/by/4.0/>).

**Keywords:** piezoelectricity; piezoelectric ceramics; 3D printing

## 1. Introduction

The piezoelectric effect was discovered by the Curie brothers in 1880 and named after the Greek word  $\pi\acute{\epsilon}\zeta\omega$  (piézēin), meaning to press. The piezoelectric effect means the mutual conversion of mechanical energy and electrical energy. It can be divided into a primary piezoelectric effect, in which electricity is generated by mechanical pressure, and a secondary piezoelectric effect, in which mechanical structural change occurs by an electrical signal.

Twenty-one of the thirty-two crystallographic point groups are not centrosymmetric, and all of them have piezoelectric properties except for one type of exception. This group of twenty crystallographic points is called piezoelectric, and quartz is a representative material. Since electricity is generated when mechanical vibration is applied to the piezoelectric material, it is widely used in manufacturing energy harvesters using the piezoelectric material [1]. Among these twenty crystallographic point groups, ten have spontaneous polarization, and the spontaneous polarization can be changed by heat. A material with this property is zinc oxide (ZnO), which is called pyroelectric. In addition, there is a material that can change the direction of spontaneous polarization by an external electric field, and this is called a ferroelectric. Ceramic materials such as lead zirconate titanate (PZT) and



## 2. Piezoelectricity

The electric displacement field and Hooke’s law can be used to explain the piezoelectric effect, which is a mix of electrical and mechanical events. The electric displacement field and Hooke’s law are:

$$D = \epsilon E \tag{1}$$

$$S = sT \tag{2}$$

$D$  is the electric displacement field,  $\epsilon$  is the permittivity, and  $E$  is the electric field.  $S$  is the strain,  $T$  is the stress, and  $s$  is the proportional constant. Combining the two equations results in an equation for the piezoelectric effect.

$$D = dT + \epsilon E \tag{3}$$

$$S = sT + d^T E \tag{4}$$

The electric displacement field and the electric field are vectors. Permittivity, strain, and stress are rank-2 tensors, and the proportional constant is the rank-4 tensor. It can be expressed without a tensor by using the symmetry of the strain and the stress tensors.

$$\begin{bmatrix} S_1 \\ S_2 \\ S_3 \\ S_4 \\ S_5 \\ S_6 \end{bmatrix} = \begin{bmatrix} S_{11}^E & S_{12}^E & S_{13}^E & 0 & 0 & 0 \\ S_{21}^E & S_{22}^E & S_{23}^E & 0 & 0 & 0 \\ S_{31}^E & S_{32}^E & S_{33}^E & 0 & 0 & 0 \\ 0 & 0 & 0 & S_{44}^E & 0 & 0 \\ 0 & 0 & 0 & 0 & S_{55}^E & 0 \\ 0 & 0 & 0 & 0 & 0 & S_{66}^E \end{bmatrix} \begin{bmatrix} T_1 \\ T_2 \\ T_3 \\ T_4 \\ T_5 \\ T_6 \end{bmatrix} + \begin{bmatrix} 0 & 0 & d_{31} \\ 0 & 0 & d_{32} \\ 0 & 0 & d_{33} \\ 0 & d_{24} & 0 \\ d_{15} & 0 & 0 \\ 0 & 0 & 0 \end{bmatrix} \begin{bmatrix} E_1 \\ E_2 \\ E_3 \end{bmatrix} \tag{5}$$

$$\begin{bmatrix} D_1 \\ D_2 \\ D_3 \end{bmatrix} = \begin{bmatrix} 0 & 0 & 0 & 0 & d_{15} & 0 \\ 0 & 0 & 0 & d_{24} & 0 & 0 \\ d_{31} & d_{32} & d_{33} & 0 & 0 & 0 \end{bmatrix} \begin{bmatrix} T_1 \\ T_2 \\ T_3 \\ T_4 \\ T_5 \\ T_6 \end{bmatrix} + \begin{bmatrix} \epsilon_{11} & 0 & 0 \\ 0 & \epsilon_{22} & 0 \\ 0 & 0 & \epsilon_{33} \end{bmatrix} \begin{bmatrix} E_1 \\ E_2 \\ E_3 \end{bmatrix} \tag{6}$$

Therefore, coefficients related to piezoelectricity can be expressed in the following four types:

$$d_{ij} = \left( \frac{\partial D_i}{\partial T_j} \right)^E = \left( \frac{\partial S_j}{\partial E_i} \right)^T \tag{7}$$

$$e_{ij} = \left( \frac{\partial D_i}{\partial S_j} \right)^E = - \left( \frac{\partial T_j}{\partial E_i} \right)^S \tag{8}$$

$$g_{ij} = - \left( \frac{\partial E_i}{\partial T_j} \right)^D = \left( \frac{\partial S_j}{\partial D_i} \right)^T \tag{9}$$

$$h_{ij} = - \left( \frac{\partial E_i}{\partial S_j} \right)^D = - \left( \frac{\partial T_j}{\partial D_i} \right)^S \tag{10}$$

where  $d_{ij}$  is the piezoelectric coefficient,  $e_{ij}$  is the piezoelectric stress coefficient,  $g_{ij}$  is the piezoelectric voltage constant, and  $h_{ij}$  is the piezoelectric stiffness constant. The piezoelectric coefficient and piezoelectric voltage constant are the most commonly used.

Table 1 shows the piezoelectric properties of several major materials.

**Table 1.** Material properties of Piezoelectric materials.

Material	Piezoelectric Coefficient [pC/N]	Piezoelectric Voltage Constant [10 <sup>-3</sup> Vm/N]	Ref.
Quartz	2.3	57.8	[3]
ZnO	12	15.2	[3]
NKN	80	31.5	[4]
BTO	190	12.6	[5]
PZT-5A	390	40	[5]
PVDF	23	216	[5]

### 3. Piezoelectric Particle Composite Dispersion

To 3D print a piezoelectric material, piezoelectric particles must be mixed with resin and produced in the form of a slurry. However, the particles have a strong tendency to aggregate together due to the clustering effect, therefore the slurry is not produced uniformly [6,7]. Generally, piezoelectric powders are mixed in a colloidal form in a resin. The behavior of piezoelectric powder is affected by the interaction of the attractive force due to the van der Waals force. The repulsive force caused by the electrostatic force and the tendency can be easily identified using the  $\zeta$  (zeta)-potential [8,9].

Zeta potential, which is the electric potential difference between the surface of a particle and the surrounding fluid or dispersant, is an important property of colloidal dispersions. It is a measure of the degree of repulsion or attraction between particles and can be used to predict the stability of the colloidal system. When a solid particle is suspended in a liquid, the surface of the particle carries a net charge due to the dissociation of surface groups or the adsorption of ions from the liquid. This charge creates an electrical double layer around the particle, consisting of a diffuse layer of ions in the liquid adjacent to the surface and a compact layer of ions on the surface. A high magnitude of zeta potential (>30 mV) indicates strong repulsion between particles, leading to a stable dispersion. On the other hand, low or zero zeta potential (<30 mV) can result in particle aggregation and sedimentation due to attractive forces. Therefore, measuring zeta potential is an important technique in the study of colloidal systems and is widely used in industries such as pharmaceuticals, food and beverages, and cosmetics.

Since aggregation between powders does not occur as the zeta potential increases, the clustering phenomenon can be prevented through powder surface treatment. The most commonly used method is a method using a dispersant, known as a surfactant [10–12].

### 4. 3D printing Technologies of Piezoelectric Materials

According to additive manufacturing (AM) processes, 3D printing technologies are classified into four categories: vat photopolymerization (stereolithography (SLA) and digital light processing (DLP)); powder bed fusion (selective laser sintering (SLS)); material jetting (inkjet printing (IJP)); and material extrusion (direct ink writing (DIW) and fused deposition modeling (FDM)). Overall, printing technologies can be selected based on resolution requirements, material types, and multi-material fabrication requirements.

#### 4.1. Vat Photopolymerization

SLA is a 3D printing technique that uses a specific wavelength, usually in the ultraviolet range, to selectively cure the photocurable resin. When the printing process begins, the resin's surface height is equal to the thickness of one layer above the vat or platform, and the laser quickly scans and solidifies the first layer of the object along a controlled direction. Objects are printed layer-by-layer in the same manner until the overall shape is complete [13]. SLA is capable of manufacturing objects with high surface quality and fine resolutions down to the micrometer-scale. Figure 2a depicts a typical SLA technique in a schematic diagram. To successfully execute the printing process, several factors must be considered, including dispersibility, viscosity, and the impact of light scattering. The material particles must be uniformly and effectively dispersed in the photopolymerizable

medium and maintain a viscosity suitable for working on suspensions of tens of Pa·s at a shear rate of  $1000\text{ s}^{-1}$  [14]. The use of piezoelectric materials in SLA has potential applications in the development of sensors, actuators, and piezoelectric ceramics [15–17]. Figure 2b illustrates an SLA-based molecularly designed photo elastomer that allows for complete self-healing [17]. The authors demonstrate the rapid AM of single- and multi-material elastomer structures with various complex 3D geometries in a short time ( $\approx 13.5\text{ mm}^3\text{ min}^{-1}$ ). Figure 2c,d shows the 3D-printed BaTiO<sub>3</sub> (BTO) ceramic array and transducers with 80% BTO ceramics produced using the SLA method [16]. A focused array of around 1.4 MHz displays a broad bandwidth of 40% at  $-6\text{ dB}$  with an insertion loss of approximately 50 dB, which indicates great potential for complex-structure ultrasonic arrays.

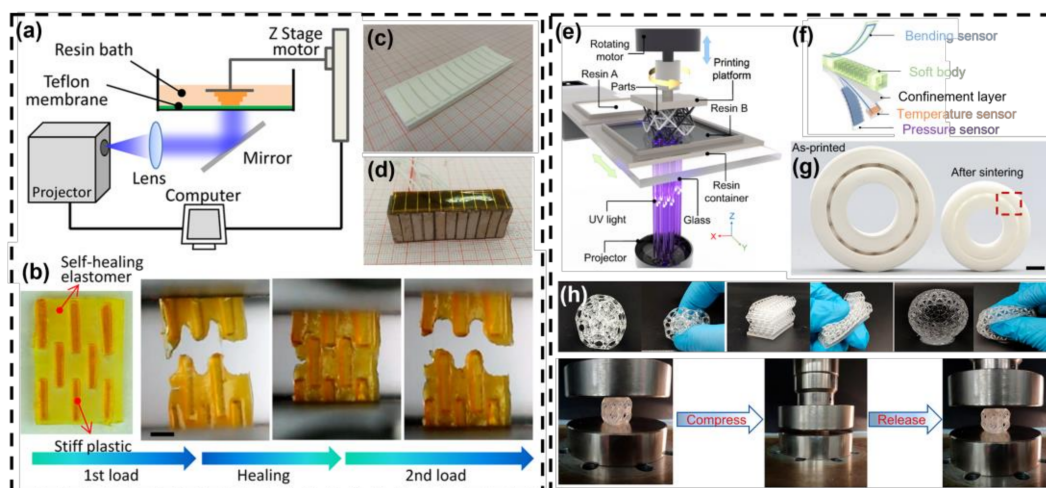


**Figure 2.** (a) SLA-based AM process. (b) Self-healable 3D soft actuator. A notched stiff-soft composite is first uniaxially stretched until a rupture and then brought into contact to heal [17] (Copyright 2019, Springer Nature Limited). The photos of the 3D-printed (c) ceramic and (d) ultrasonic arrays are presented in [16] (Copyright 2019, MDPI). (e) A bottom-up DLP printing system. Printed (f) soft actuator with multiple sensors and (g) ceramic bearing [18] (Copyright 2022, Springer Nature). (h) 3D-printed hollow 3D structure for stretchable electronic sensors and a printed organic frame undergoing a compressive strain [19] (Copyright 2020, American Chemical Society).

The main difference between SLA and DLP is that SLA uses a point-source laser beam, while DLP projects images onto the entire platform at each layer to increase printing speed [20]. As the printing is conducted upside down in DLP, complex structures can be formed without needing supporting material. Among DLP techniques, projection micro-stereolithography (PμSL) has achieved higher resolution (up to  $0.6\text{ }\mu\text{m}$ ) through improvements in layer thickness control and exposure correction [21]. Figure 2e shows a schematic diagram of the DLP technique. However, traditional DLP methods are not suitable for multi-material 3D printing, as multi-material printing methods require direct contact with the printed part to remove residual resin [18]. The use of piezoelectric materials in DLP printing can improve printing speed and precision, as well as enable the creation of more intricate structures. Potential applications of this technology include the development of sensors, micro-electromechanical systems (MEMS), and optical components [19,22]. Figure 2f,g shows the printed soft actuator and ceramic bearings using a DLP-based centrifugal multi-material (CM) 3D printing method to generate large-volume, heterogeneous 3D objects, in which composition, property, and function are programmable at the voxel scale [18]. The CM 3D printing system enables direct printing of a soft pneumatic actuator where bending, pressure, and temperature sensors are seamlessly integrated (Figure 2f). To demonstrate the technology's impact on engineering parts manufacturing, the authors design a ceramic bearing that requires empty space between the rollers and the inner/outer rings to enable free rotation (Figure 2g). To support these freestanding rollers, the authors design and print elastomers to fill the empty space. The sintering process removes the elastomer, which

allows the ball bearing to rotate freely without resistance. The CM 3D printing method complements the limitations of conventional DLP technology and substantially enhances multi-material 3D printing capabilities for creating multi-functional heterogeneous objects. In Figure 2h, the authors successfully synthesized three types of poly(urethane acrylate) oligomers and used them to prepare resins (PUAs-40) with low viscosity for a common DLP printer without custom equipment. Various complex 3D objects, such as a lattice structure, a hyper-small soccer ball, and an organic frame, were constructed [19]. The 3D object remained intact after 100 cycles of 80% strain compression, which demonstrates its high compressibility and durability.

#### 4.2. Powder Bed Fusion

SLS uses thermal energy from a high-power laser to selectively irradiate the surface of a target powder bed, building a 3D structure. The process involves sintering or fusing powder particles with a laser to create a solid structure [23]. The SLS technique can achieve isotropic mechanical properties in the printed object, and no extra support structures are needed for overhanging regions. Figure 3a shows a schematic diagram of the SLS process. While SLS systems can be expensive, they have been reported as suitable techniques for high-quality piezoelectric elements and ceramics [24]. For achieving the desired piezoelectric properties, it is critical to carefully consider the processing parameters, crystal orientation control, and post-processing, such as annealing or polishing. SLS printing has a wide range of applications, including accelerometer sensors, piezoelectric ceramics, and energy harvesting devices [25–27]. Piezoelectric energy harvesters with micropore construction were fabricated using SLS and supercritical carbon dioxide foaming (Sc-CO<sub>2</sub>) technologies, as shown in Figure 3b [26]. The prepared foam could directly produce 19.3 V and 415 nA electrical output, surpassing most of the PVDF piezoelectric energy harvesters reported thus far (Figure 3c).

#### 4.3. Material Jetting

IJP is a well-known non-contact printing method for creating patterns by ejecting ink droplets through printhead nozzles onto a substrate [28]. Binder jetting and polymer jetting are two key processes in IJP. In binder jetting, the binder is selectively dispensed onto the powder bed to create a cross-section of the object. In polymer jetting, the inkjet printhead deposits photosensitive polymer onto the substrate, which is then cured by a light source. Figure 3d shows a schematic diagram of IJP for printing. IJP is primarily used for printing electronics because it can print complex patterns with a wide range of materials at high resolution. However, it has limited flexibility in complex structure design, such as hollow structures or the inability to print overhanging structures due to difficulties with support preparation [14]. Growing interest has been shown in further applications of IJP for 3D piezoelectric and ceramic parts, especially for the fabrication of functional components used in microelectronics [29–31]. Figure 3e demonstrates the applicability of the developed IJP printhead to the deposition of ceramic suspensions and concentrated polymer solutions by successfully jetting a ZnO suspension and a poly(3,4-ethylenedioxythiophene) (PEDOT)-based solution [30]. The use of ZnO nanoparticle suspension suggests possible applications in the jetting of ceramics for sensing or microelectronic applications. Figure 3f presents an electromagnetically driven actuator, fully developed by low-cost IJP technology [31]. This actuator can be suitably applied for positioning applications in the millimeter range with a required loading in the order of hundreds of  $\mu\text{N}$ .

#### 4.4. Material Extrusion

DIW uses direct material deposition and operates by extruding a paste-like ink with shear-thinning properties [32]. It is suitable for a wide range of materials, from very low-viscosity solutions to very high-viscosity plastic-like materials. The object is created by directly “writing” the shape designed for each layer by moving the nozzle until the part is completed. The parts are then degreased and sintered to remove organics. Figure 3g

shows a schematic diagram of DIW. There are several challenges associated with printing piezoelectric materials using DIW. The printing process itself can introduce stresses and defects that can affect the performance of the material. Additionally, the ink must be carefully formulated to ensure that the printed structures have the desired piezoelectric properties. The advantage of DIW is its ability to fabricate free-standing structures with spanning parts without supports or high aspect ratio walls, which are not possible with other 3D printing technologies. DIW-based woodpile lattice structures and small electronic components have shown considerable promise, particularly around bandgap structures such as photonic crystals and piezoelectric components such as transducers [33,34]. Figure g presents an example of an underwater acoustic transducer fabricated via lead zirconate titanate (PZT) piezoelectric composites and DIW combined with furnace sintering and resin impregnation [33]. The electrical signal generated by the underwater acoustic transducer changed autonomously with the acoustic stimulation, indicating great potential for underwater detection and communication applications.

FDM is a 3D printing technology that uses a thermoplastic material to create a physical object. FDM works by melting a thermoplastic filament and extruding it through a heated nozzle. The nozzle moves in a predetermined pattern, laying down layers of the melted material, which then solidify as they cool. A schematic diagram of the FDM process is depicted in Figure 3h. FDM is the cheapest, simplest, most accessible, and environmentally friendly 3D printing method. However, the printable materials are limited, and the resolution is generally low compared to other printing methods. In the case of ceramics, this is because the nozzle of FDM tends to be rather large [35]. The viscosity of the fused filaments should generally be in the range of 10 to 100 Pa·s. Additionally, the piezoelectric/ceramic particles should be well dispersed in the filament to obtain a constant and stable flow [34]. Growth in potential applications lies in the fabrication of functional electronic components such as transducers and sensors [36,37]. Figure 3i shows an FDM-printed capacitive interface [38]. To use the printed device, a user touches the printed conductive pad; the capacitance of the pad increases, which is then sensed by the Arduino board and used to trigger an operation. This approach will open up many new applications for FDM where fully interactive devices can be printed.

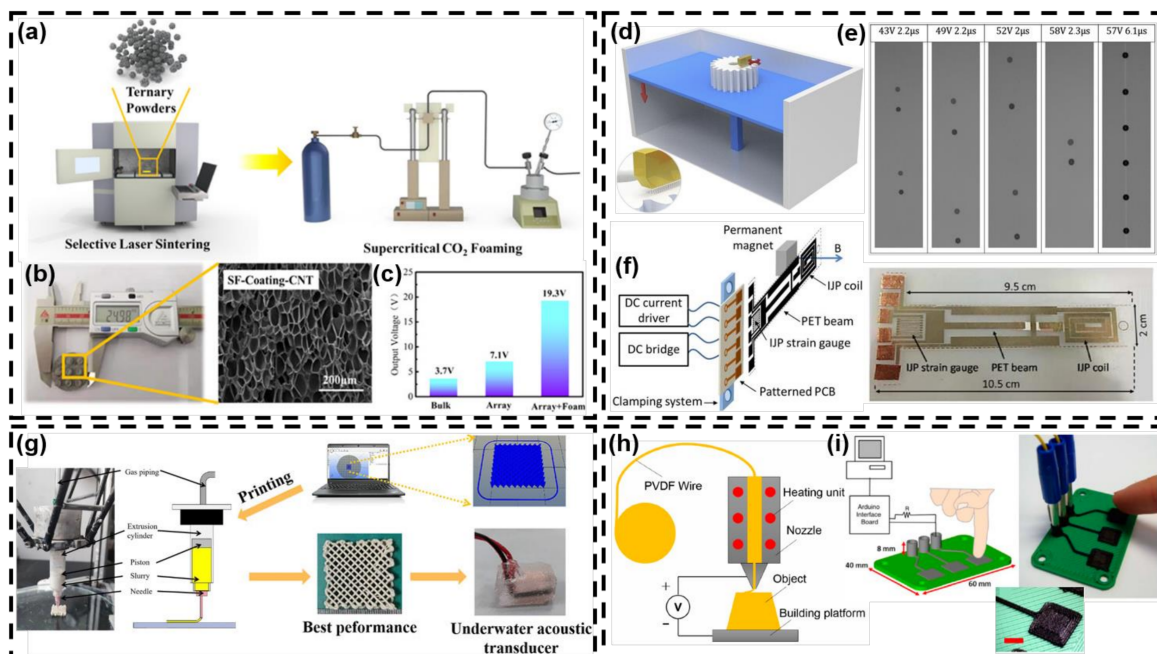


**Figure 3.** (a) Preparation of SLS-based porous foam. (b) Printed energy harvester and scanning electron microscopy (SEM) image of pore morphologies. (c) Output of a piezoelectric energy harvester [26] (Copyright 2021, American Chemical Society). (d) IJP process with inset showing the printhead jetting

droplets [14] (Copyright 2019, Elsevier). (e) Jetting in different conditions through a printhead design [30] (Copyright 2021, John Wiley and Sons). (f) Schematization of the IJP actuator and real view of the device [31] (Copyright 2016, MDPI). (g) The fabrication route of DIW underwater acoustic transducers [33] (Copyright 2021, Frontiers). (h) Electric poling-assisted FDM process [34] (Copyright 2018, MDPI). (i) FDM-printed capacitive sensor [38] (Copyright 2012, PLOS).

The advantages, disadvantages, and applications of 3D printing technologies are described in Table 2.

**Table 2.** Advantages, disadvantages, and applications of the most used 3D printing technologies.

Method	Advantages	Disadvantaged	Application	Ref.
SLA	Simple and rapid fabrication, a wide variety of applications, high precision, ability to produce complicated structures with great features details	High-cost technology, the support materials should be removed, and single material limits cationic photopolymerization resins	Piezoelectric pressure sensor, ultrasonic transducer, self-healable actuator, piezoelectric ceramic	[15–17]
DLP	High resolution, fast printing speed, large build volume, a wide range of materials, high precision, and accuracy	Expensive equipment, requires post-processing, limited lifespan of the resin tank	Piezoresistive strain sensor, piezoelectric microphone, capacitive pressure sensor	[18,19,22]
SLS	Self-sustaining process, strong and precise parts, lower cost materials if used in large volume, no need for support material	Inhalation risk, limited mechanical properties, rough surface and required elaborate post-processing (for metals), messy powders, and high cost	Piezoelectric ceramic, mechanical energy harvester, piezoelectric accelerometer sensor	[25–27]
IJP	Wide range of materials, high-resolution structure	Specific requirements for the printable ink, low areal capacity, lack of structural diversities	Piezoelectric actuator, microelectronic (biomedicine and ceramics manufacturing)	[29–31]
DIW	High printing resolution, easy operation, strong design ability, versatility, complex multiscale architectures, low cost, a wide range of materials, diverse structures	Necessity of preparing printing inks with high rheological qualities to make printing work smoothly and requires post-processing	Acoustic transducer, complex piezoelectric ceramics, piezoelectric tactile sensor	[33,34]
FDM	High porosity, multi-material structures, variable mechanical strength, low-cost materials	Narrow printable materials range, metal materials, high cost for metal and glass materials	Piezoelectric transducer, capacitive sensor, flexible strain sensor	[36–38]

## 5. Piezoelectric Ceramics for 3D Printing

Piezoelectric ceramics have a higher piezoelectric constant (hundreds of pC/N) than piezoelectric polymers (~30 pC/N), making them advantageous in terms of piezoelectric properties for 3D printing [39]. However, a limitation of the traditional ceramic synthesis method is that complex shapes cannot be created since uniaxial pressing is typically used. Recently, as research on the application of piezoelectric materials has become more active, there has been a growing need for complex-shaped piezoelectric elements. Consequently, various research results and review papers on the 3D printing of piezoelectric ceramics have been published. In this section, we will review the 3D printing methods and results for representative piezoelectric ceramics such as PZT (Pb(Zr,Ti)O<sub>3</sub>), PMN-PT (Pb(Mg,Nb,Ti)O<sub>3</sub>), BTO (BaTiO<sub>3</sub>), and NKN ((Na,K)NbO<sub>3</sub>). Slurry-based ceramic 3D printing technology uses a liquid system dispersed with ceramic particles as feedstock and can be 3D printed using photopolymerization, inkjet printing, and extrusion methods. In addition to the slurry preparation additives and the piezoelectric properties of the ceramics, the particle size and fraction of the piezoelectric ceramics are also important factors in controlling the dispersion and viscosity of the slurry [40–42]. Therefore, as shown in Table 3, we presented the additives, particle sizes, and contents of the piezoelectric ceramics, as well as the density and piezoelectric properties ( $d_{33}$  and  $\epsilon_r$ ) after sintering.

### 5.1. Lead-Based Piezoelectric Ceramics

Since the discovery of PZT in the 1950s, it has been widely studied and commercialized due to its high piezoelectric properties [43]. The PZT is a solid solution of PbTiO<sub>3</sub> and

$\text{PbZrO}_3$ . It is known to show the highest piezoelectric properties at the MPB (Morphotropic Phase Boundary) phase, which is the boundary between the rhombohedral phase and the tetragonal phase [44,45]. In addition, the PZT has a perovskite structure of  $\text{ABO}_3$ , and various piezoelectric parameters such as curie temperature, permittivity, and piezoelectric constant can be adjusted by substituting dopants for A- and B-sites. When donor material is doped, it changes into a “soft” piezoelectric material with a large piezoelectric constant value. This is because oxygen vacancy makes domain wall motion easier. Conversely, if the acceptor is doped, the oxygen vacancy pins the domain wall motion, resulting in the characteristics of a “hard” piezoelectric material with reduced loss. Soft piezoelectric materials are mainly used for actuators, sensors, and energy harvesting, whereas hard piezoelectric materials are used for ultrasonic applications that require high power.

Furthermore, PZT is widely used as a raw material for 3D printing and has been extensively studied by researchers. Hu et al. used the SLA method and the burnable plastic sphere (BURPS) technique to 3D print PZT structures [46], as shown in Figure 4a–d. They prepared a printing slurry by mixing photocurable ceramic suspensions with polymethylmethacrylate (PMMA) as a pore-forming agent and confirmed that the curing depth increased with increasing PMMA content. The sintered PZT ceramics exhibited electrical and piezoelectric properties comparable to those fabricated by conventional methods. This suggests that SLA can be an effective tool for producing ceramic components with complex geometric structures.

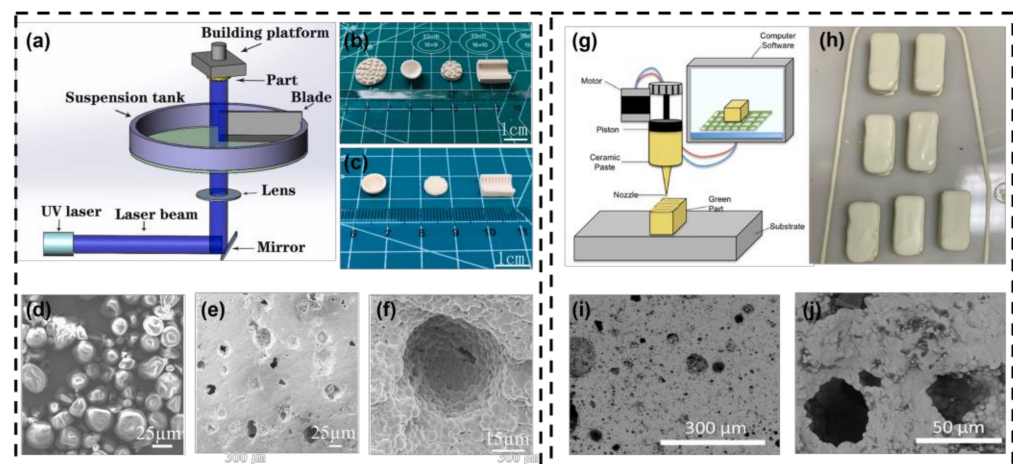


**Figure 4.** (a) The schematic of the SLA technique for 3D printing of PZT ceramics. Images of the 3D-printed ceramic arrays with various complex structures of (b) printed green bodies and (c) sintered ceramic parts. The SEM images of (d) PMMA particles, (e) surface morphology of the porous PZT ceramics fabricated by the SLA technique, and (f) magnified microstructure of a spherical pore [46] (Copyright 2021, Elsevier). (g) The schematic of the DIW method for PZT ceramics, (h) fabricated PZT ceramic green bodies, and the SEM images displaying (i) the top surface and (j) the cross-section of sintered samples [47] (Copyright 2021, Elsevier).

Hall et al. also 3D printed PZT ceramics using the DIW method [47], as shown in Figure 4e–i. They reported that the piezoelectric properties of the PZT ceramics synthesized by traditional methods and those printed using the DIW method were not significantly different. However, the printed images revealed a lower resolution compared to the previously mentioned SLA method. This suggests that the SLA method, which involves photocuring, is more advantageous than the DIW method, which involves directly extruding ink when it comes to creating complex shapes.

Since the 1980s, when PMN was first identified as a relaxor-ferroelectric material, research on the composition of PMN-PT with outstanding piezoelectric properties has been conducted [48,49]. The excellent piezoelectric properties of relaxor-PT is explained by the domain structure composed of polar nanoregions (PNR). It is believed that the reason for the outstanding piezoelectric properties is due to the domain reacting more sensitively to

external stimuli than the classical ferroelectric domain [50]. Due to its exceptional piezoelectric properties, research has been conducted using relaxor-PT as a raw material for piezoelectric 3D printing, as shown in Figure 5a–c.

### 5.2. Lead-Free Piezoelectric Ceramics

The BTO was the first perovskite piezoelectric material discovered and was used as sonar in World War II [51]. However, with the discovery of PZT, its use is limited due to its relatively low piezoelectric properties and temperature stability. Nevertheless, as environmental concerns have increased, the issue of lead has emerged [52]. For this reason, research on lead-free piezoelectric ceramics such as BTO and NKN to replace lead-based materials is actively being conducted. NKN ceramics are considered one of the most promising candidates for replacing lead-based piezoelectric ceramics due to their high curie temperature and piezoelectric properties [53].

However, obtaining dense ceramics is difficult due to the high deliquescence and volatility of  $K_2CO_3$ . Consequently, research is being conducted to manufacture high-density piezoelectric ceramics using various methods, such as RTGG and hot pressing [54]. Due to the difficulties in sintering, creating complex shapes using 3D printing with lead-free piezoelectric ceramics is known to be more challenging compared to lead-based materials for achieving high piezoelectric properties. Nevertheless, it is being actively studied as a raw material for 3D printing that is environmentally friendly, as shown in Figure 5d,e and Table 3.

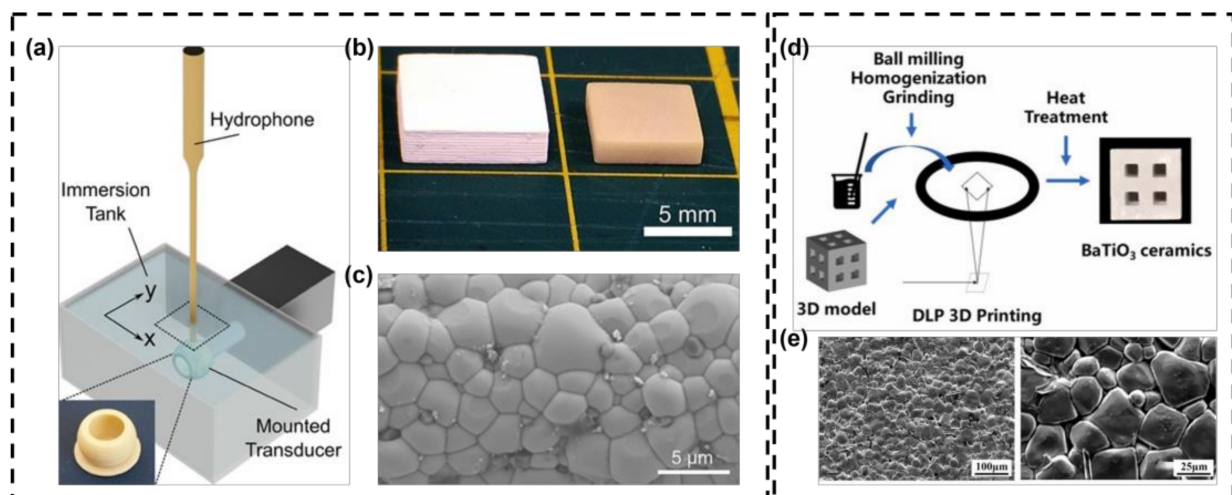


**Figure 5.** The 3D printing of two types of piezoelectric ceramics. (a) The schematic of an SLA 3D printing system for PMN-PT, (b) PMN-PT piezoelectric ceramics embedded within the polymer matrix (left), the corresponding sintered sample (right), and (c) the grain structure of the sintered sample [55] (Copyright 2015, John Wiley and Sons). (d) the schematic of the DLP 3D printing system employed to produce BTO ceramics. (e) The grain structure of sintered BTO ceramics [56] (Copyright 2022, Elsevier).

### 5.3. Application of 3D Printed Piezoelectric Ceramics

The use of a focused piezoelectric element is common in ultrasonic defectoscope (nondestructive testing), ultrasonic imaging, and high-intensity focused ultrasound (HIFU) because it provides high sensitivity and smaller lateral resolution [57]. Typically, these elements are machined to achieve the necessary focusing features. However, the machining process can cause cracking and ferroelastic domain reorientation, which in turn can increase the loss of tangent and decrease the working life of the piezoelectric layer. This effect is not observed in materials that have not undergone the machining process. Therefore, many studies using 3D printing methods in high-power applications such as ultrasonic transducers have been reported [16,58–60].

Chen et al. fabricated a structure that enables energy focusing and ultrasonic sensing by printing a transducer using piezo-composite slurry through the stereolithography (SLA) method [59], as shown in Figure 6. The performance of the transducer was tested using an ultrasonic system, and the beam profile was predicted by the Field II program (Figure 6b). The original pulse and the echo that were produced by the focused transducer when the depth between the transducer and the quartz target was 5 mm (Figure 6c). The pulse and echo demonstrate that the 3D-printed ceramics can convert compressive and tensile stresses into an electric charge and vice versa (Figure 6d).

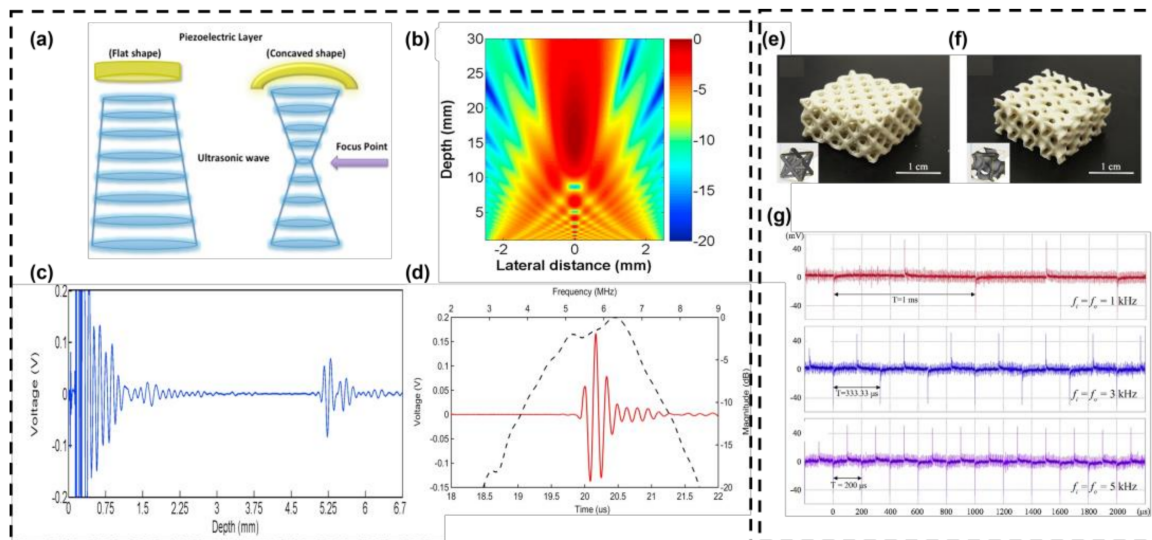


**Figure 6.** (a) The schematic diagram of the non-focused and focused transmit beam generated by the ultrasonic transducer. (b) Beam profile simulation by Field II program. (c) Initial pulse and echo generated by the printing-focused transducer. (d) Pulse-echo waveform (solid line) and normalized spectrum [59]. (e,f) The complex-structured BTO ceramics and composites are fabricated by the DLP process. (g) The output signal waveforms when changing the input signal frequency [61].

Liu et al. reported the stereolithography-based 3D printing method for barium titanate (BTO), which utilizes a high refractive index monomer to improve curing ability [61]. Furthermore, complex-structured ceramics and functional devices such as hydrophones were successfully manufactured using DLP 3D printing with piezoelectric composites of octet-truss and gyroid structures, demonstrating the feasibility of this approach, as shown in Figure 6e and f. The hydrophone was tested by measuring the waveforms produced under various square wave input signals, as shown in Figure 6f. The results showed that as the frequency of the input signal ( $f_i$ ) changed within the range of 1–5 kHz, the frequency of the output signal ( $f_o$ ) also changed proportionally, while the magnitude remained constant. This confirms that the hydrophone can receive signals.

**Table 3.** Comparison of piezoelectric ceramics 3D printing.

Material	Fabrication Method	Additive	Ceramic Contents	Grain Size	Measured Density (g/cm <sup>3</sup> )	Relative Density (%)	Piezoelectric Coefficient (pC/N)	Relative Permittivity A. U.	Ref.
PZT	SLA	Photosensitive resin	82 wt%	500 nm	6.99		345	1040	[58]
		TMSPM, Ultraviolet-sensitive monomer	72 wt%	220.9 nm			110		[12]
		Negatively charged resin, SiOC monomer	50 vol%				583		[62]
	DIW	Polyvinyl alcohol coating + DI Water	86 wt%	500 nm	7.21	94.9	678	4132	[47]
PMN-PT	SLA	Photocurable resin (HDDA, DPPHA, BASF)	40 vol%	2 µm	7.98	97.8	620		[55]
	DLP	Photopolymer grey resin	60 wt%	5 µm			67		[63]
BTO	SLA	Photosensitive resin	80 wt%	500 nm	5.65	93.9	166	2177	[16]
		MEK + Ethanol, Phopholan PS-131, Triton x-100, photocurable resin (SI500)	80 wt%	1 µm	5.7	95	87	920	[64]
		MEK + Ethanol, Phopholan PS-131, Triton x-100, photocurable resin (SI500)	70 wt%	100 nm	5.64	93.7	160	1350	[59]
		Photopolymer resin (SG 15), PT-MR 10-35GT dispersant	70 wt%	1.02 µm	5.44	90	200	1965	[65]
	DLP	Acrylic resin, Camphor quinone, Parbenate, Triethanolamine, Tetraethyl orthosilicate	80 wt%	100 nm	5.72	94.2	241		[56]
		Triton X-100, MPDISP, ACOMO, TPO, MEHQ, Epoxy resin, PDMS	80 wt%	993 nm	5.74	95.3	168	1512	[40]
	IJP	Binder	40 vol%	0.85~1.45 µm	3.93	65.3	74.1	640	[60]
	DIW	PVDF, DMF	77 wt%	500 nm	3.93	65.3	200	4730	[66]
NKN	SLA	Triton x-100, Photocurable resin (Acrylamide monomer, Diphenyl phosphine oxide)	65 wt%	400 nm	4.09	92	170	2150	[67]
	IJP	Organic binder (BA005)		100~500 nm	2.5	55.6	84.8		[68]
	DIW	Methyl methacrylate, pentaerythritol three acrylate	56 wt%	500 nm	4.52	98	280	1775	[69]

## 6. Conclusions

In conclusion, we introduced various methods and materials for the 3D printing of piezoelectric ceramics and focused on the conditions for successful printing. For 3D printing, proper powder size and surface treatment for uniform dispersion are important. In addition, as discussed above, the advantages and disadvantages of each 3D printing method are clear, and suitable applications are different. Therefore, it is essential to select a suitable 3D printer according to the application field.

SLA and DLP are two 3D printing techniques that use specific wavelengths to selectively cure photocurable resin layer-by-layer. SLA is capable of manufacturing high-quality objects with fine resolutions, while DLP can create complex structures without needing supporting material. SLS uses a laser to selectively sinter or fuse powder particles to create a solid structure without support structures for overhanging regions. It can achieve isotropic mechanical properties and is suitable for high-quality piezoelectric elements and ceramics. IJP is a non-contact printing method that ejects ink droplets through printhead nozzles onto a substrate. It has limited flexibility in complex structure design but is suitable for printing electronics and is increasingly used for 3D piezoelectric and ceramic parts in microelectronics. Direct ink writing (DIW) is a 3D printing technology that extrudes a paste-like ink with shear-thinning properties, suitable for a wide range of materials. DIW can fabricate free-standing structures without supports or high aspect ratio walls and has shown promise in creating piezoelectric components such as transducers. Fused deposition modeling (FDM) is the cheapest and most accessible 3D printing method but has limitations in printable materials and resolution. Due to their high sensitivity and small lateral resolution, piezoelectric elements are often used in ultrasound imaging, nondestructive testing, and high-intensity focused ultrasound. However, machining these elements to achieve the necessary focusing features can cause cracking and ferroelastic domain reorientation, which can lead to a shorter working life. To address this issue, many researchers have used 3D printing methods to manufacture piezoelectric transducers. These 3D-printed ceramics have shown the capacity to convert compressive and tensile stresses into an electric charge and vice versa, confirming their potential use as sensors.

While 3D printing of piezoelectric materials shows promise in increasing their performance and applications, there are still several challenges and limitations to be addressed. One of the main challenges is the porosity of 3D-printed piezoelectric ceramics, which makes it difficult to produce a dense structure. Additionally, the rate of damage during production is higher than that of the press method. Furthermore, the materials used for 3D printing may not have the same properties as conventionally processed piezoelectric ceramics, which can impact their performance. Another limitation is the limited size and shape of the piezoelectric elements that can be printed, which restricts their use in certain applications. Despite these challenges, research in this field is ongoing, and there is hope that these limitations can be overcome, leading to more progress in piezoelectric technology.

**Author Contributions:** J.P. and D.-G.L. contributed equally to this work. Conceptualization; J.P., D.-G.L., H.S.K. and H.-C.S.; writing—original draft preparation, J.P., D.-G.L. and H.S.K.; writing—review and editing, J.P., D.-G.L. and H.S.K.; visualization, J.P. and D.-G.L.; supervision, S.H., J.M.B., H.S.K. and H.-C.S.; project administration, H.-C.S.; funding acquisition, H.-C.S.; All authors have read and agreed to the published version of the manuscript.

**Funding:** The authors acknowledge that this work was supported by the National Research Foundation (NRF) of Korea funded by the Ministry of Education (grant numbers NRF-2021R1C1C1009100 and NRF-2020M3H4A3105594), and the Korea Institute of Science and Technology (KIST) (grant numbers 2E32491 and 2V09793).

**Data Availability Statement:** Not applicable.

**Conflicts of Interest:** The authors declare no conflict of interest.

## References

1. Lee, D.-G.; Shin, J.; Kim, H.S.; Hur, S.; Sun, S.; Jang, J.-S.; Chang, S.; Jung, I.; Nahm, S.; Kang, H.; et al. Autonomous Resonance-Tuning Mechanism for Environmental Adaptive Energy Harvesting. *Adv. Sci.* **2023**, *10*, 2205179. [[CrossRef](#)] [[PubMed](#)]
2. Kim, H.S.; Hur, S.; Lee, D.-G.; Shin, J.; Qiao, H.; Mun, S.; Lee, H.; Moon, W.; Kim, Y.; Baik, J.M.; et al. Ferroelectrically Augmented Contact Electrification Enables Efficient Acoustic Energy Transfer through Liquid and Solid Media. *Energy Environ. Sci.* **2022**, *15*, 1243–1255. [[CrossRef](#)]
3. Forero-García, E.F.; Gélvez-Lizarazo, Ó.M.; Torres-Pinzón, C.A. Piezoelectric Transducer Design for Electric Power Generation. *Rev. UIS Ing.* **2019**, *18*, 119–126. [[CrossRef](#)]
4. Jaeger, R.E.; Egerton, L. Hot Pressing of Potassium-Sodium Niobates. *J. Am. Ceram. Soc.* **1962**, *45*, 209–213. [[CrossRef](#)]
5. Boukabache, H.; Escriba, C.; Fourniols, J.-Y. Toward Smart Aerospace Structures: Design of a Piezoelectric Sensor and Its Analog Interface for Flaw Detection. *Sensors* **2014**, *14*, 20543–20561. [[CrossRef](#)]
6. Kim, H.; Lee, D.; Kim, D.; Kong, D.; Choi, J.; Lee, M.; Murillo, G.; Jung, J. Dominant Role of Young's Modulus for Electric Power Generation in PVDF–BaTiO<sub>3</sub> Composite-Based Piezoelectric Nanogenerator. *Nanomaterials* **2018**, *8*, 777. [[CrossRef](#)]
7. Stolarczyk, J.K.; Deak, A.; Brougham, D.F. Nanoparticle Clusters: Assembly and Control Over Internal Order, Current Capabilities, and Future Potential. *Adv. Mater.* **2016**, *28*, 5400–5424. [[CrossRef](#)]
8. Uskoković, V. Dynamic Light Scattering Based Microelectrophoresis: Main Prospects and Limitations. *J. Dispers. Sci. Technol.* **2012**, *33*, 1762–1786. [[CrossRef](#)]
9. Marsalek, R. Particle Size and Zeta Potential of ZnO. *APCBEE Procedia* **2014**, *9*, 13–17. [[CrossRef](#)]
10. Kim, K.; Zhu, W.; Qu, X.; Aaronson, C.; McCall, W.R.; Chen, S.; Sirbulu, D.J. 3D Optical Printing of Piezoelectric Nanoparticle–Polymer Composite Materials. *ACS Nano* **2014**, *8*, 9799–9806. [[CrossRef](#)]
11. Gonzalez, G.; Chiappone, A.; Roppolo, I.; Fantino, E.; Bertana, V.; Perrucci, F.; Scaltrito, L.; Pirri, F.; Sangermano, M. Development of 3D Printable Formulations Containing CNT with Enhanced Electrical Properties. *Polymer* **2017**, *109*, 246–253. [[CrossRef](#)]
12. Cui, H.; Hensleigh, R.; Yao, D.; Maurya, D.; Kumar, P.; Kang, M.G.; Priya, S.; Zheng, X. Three-Dimensional Printing of Piezoelectric Materials with Designed Anisotropy and Directional Response. *Nat. Mater.* **2019**, *18*, 234–241. [[CrossRef](#)]
13. del Barrio, J.; Sánchez-Somolinos, C. Light to Shape the Future: From Photolithography to 4D Printing. *Adv. Opt. Mater.* **2019**, *7*, 1900598. [[CrossRef](#)]
14. Chen, Z.; Li, Z.; Li, J.; Liu, C.; Lao, C.; Fu, Y.; Liu, C.; Li, Y.; Wang, P.; He, Y. 3D Printing of Ceramics: A Review. *J. Eur. Ceram. Soc.* **2019**, *39*, 661–687. [[CrossRef](#)]
15. Kim, H.; Manriquez, L.C.D.; Islam, M.T.; Chavez, L.A.; Regis, J.E.; Ahsan, M.A.; Noveron, J.C.; Tseng, T.-L.B.; Lin, Y. 3D Printing of Polyvinylidene Fluoride/Photopolymer Resin Blends for Piezoelectric Pressure Sensing Application Using the Stereolithography Technique. *MRS Commun.* **2019**, *9*, 1115–1123. [[CrossRef](#)]
16. Cheng, J.; Chen, Y.; Wu, J.-W.; Ji, X.-R.; Wu, S.-H. 3D Printing of BaTiO<sub>3</sub> Piezoelectric Ceramics for a Focused Ultrasonic Array. *Sensors* **2019**, *19*, 4078. [[CrossRef](#)]
17. Yu, K.; Xin, A.; Du, H.; Li, Y.; Wang, Q. Additive Manufacturing of Self-Healing Elastomers. *NPG Asia Mater.* **2019**, *11*, 7. [[CrossRef](#)]
18. Cheng, J.; Wang, R.; Sun, Z.; Liu, Q.; He, X.; Li, H.; Ye, H.; Yang, X.; Wei, X.; Li, Z.; et al. Centrifugal Multimaterial 3D Printing of Multifunctional Heterogeneous Objects. *Nat. Commun.* **2022**, *13*, 7931. [[CrossRef](#)]
19. Peng, S.; Li, Y.; Wu, L.; Zhong, J.; Weng, Z.; Zheng, L.; Yang, Z.; Miao, J.-T. 3D Printing Mechanically Robust and Transparent Polyurethane Elastomers for Stretchable Electronic Sensors. *ACS Appl. Mater. Interfaces* **2020**, *12*, 6479–6488. [[CrossRef](#)]
20. Jiang, Y.; Islam, M.d.N.; He, R.; Huang, X.; Cao, P.; Advincula, R.C.; Dahotre, N.; Dong, P.; Wu, H.F.; Choi, W. Recent Advances in 3D Printed Sensors: Materials, Design, and Manufacturing. *Adv. Mater. Technol.* **2023**, *8*, 2200492. [[CrossRef](#)]
21. Sun, C.; Fang, N.; Wu, D.M.; Zhang, X. Projection Micro-Stereolithography Using Digital Micro-Mirror Dynamic Mask. *Sens. Actuators A Phys.* **2005**, *121*, 113–120. [[CrossRef](#)]
22. Tiller, B.; Reid, A.; Zhu, B.; Guerreiro, J.; Domingo-Roca, R.; Curt Jackson, J.; Windmill, J.F.C. Piezoelectric Microphone via a Digital Light Processing 3D Printing Process. *Mater. Des.* **2019**, *165*, 107593. [[CrossRef](#)]
23. Mazzoli, A. Selective Laser Sintering in Biomedical Engineering. *Med. Biol. Eng. Comput.* **2013**, *51*, 245–256. [[CrossRef](#)] [[PubMed](#)]
24. Lupone, F.; Padovano, E.; Ostrovskaya, O.; Russo, A.; Badini, C. Innovative Approach to the Development of Conductive Hybrid Composites for Selective Laser Sintering. *Compos. Part A Appl. Sci. Manuf.* **2021**, *147*, 106429. [[CrossRef](#)]
25. Guo, D.; Li, L.; Cai, K.; Gui, Z.; Nan, C. Rapid Prototyping of Piezoelectric Ceramics via Selective Laser Sintering and Gelcasting. *J. Am. Ceram. Soc.* **2004**, *87*, 17–22. [[CrossRef](#)]
26. Yang, C.; Song, S.; Chen, F.; Chen, N. Fabrication of PVDF/BaTiO<sub>3</sub>/CNT Piezoelectric Energy Harvesters with Bionic Balsa Wood Structures through 3D Printing and Supercritical Carbon Dioxide Foaming. *ACS Appl. Mater. Interfaces* **2021**, *13*, 41723–41734. [[CrossRef](#)]
27. Gutiérrez, N.; Galvín, P.; Lasagni, F. Low Weight Additive Manufacturing FBG Accelerometer: Design, Characterization and Testing. *Measurement* **2018**, *117*, 295–303. [[CrossRef](#)]
28. Singh, M.; Haverinen, H.M.; Dhagat, P.; Jabbour, G.E. Inkjet Printing-Process and Its Applications. *Adv. Mater.* **2010**, *22*, 673–685. [[CrossRef](#)]
29. Bucciarelli, A.; Reddy Chandraiahgari, C.; Adami, A.; Mulloni, V.; Lorenzelli, L. Precise Dot Inkjet Printing Thought Multifactorial Statistical Optimization of the Piezoelectric Actuator Waveform. *Flex. Print. Electron.* **2020**, *5*, 045002. [[CrossRef](#)]

30. Bernasconi, R.; Brovelli, S.; Viviani, P.; Soldo, M.; Giusti, D.; Magagnin, L. Piezoelectric Drop-On-Demand Inkjet Printing of High-Viscosity Inks. *Adv. Eng. Mater.* **2022**, *24*, 2100733. [[CrossRef](#)]
31. Andò, B.; Marletta, V. An All-InkJet Printed Bending Actuator with Embedded Sensing Feature and an Electromagnetic Driving Mechanism. *Actuators* **2016**, *5*, 21. [[CrossRef](#)]
32. Lewis, J.A. Direct Ink Writing of 3D Functional Materials. *Adv. Funct. Mater.* **2006**, *16*, 2193–2204. [[CrossRef](#)]
33. Liu, K.; Zhang, Q.; Zhou, C.; Shi, Y.; Sun, C.; Sun, H.; Yin, C.; Hu, J.; Zhou, S.; Zhang, Y.; et al. 4D Printing of Lead Zirconate Titanate Piezoelectric Composites Transducer Based on Direct Ink Writing. *Front. Mater.* **2021**, *8*, 659441. [[CrossRef](#)]
34. Liu, C.; Huang, N.; Xu, F.; Tong, J.; Chen, Z.; Gui, X.; Fu, Y.; Lao, C. 3D Printing Technologies for Flexible Tactile Sensors toward Wearable Electronics and Electronic Skin. *Polymers* **2018**, *10*, 629. [[CrossRef](#)]
35. Bakhtar, L.J.; Abdoos, H.; Rashidi, S. A Review on Fabrication and in Vivo Applications of Piezoelectric Nanocomposites for Energy Harvesting. *J. Taiwan Inst. Chem. Eng.* **2022**, 104651. [[CrossRef](#)]
36. Mohamed, A.S.; Maidin, S.; Mohamed, S.B.; Muhamad, M.K.; Wong, J.H.U.; Romlee, W.F.A. Improvement of Surface Finish by Multiple Piezoelectric Transducers in Fused Deposition Modelling. *Int. J. Adv. Sci. Eng. Inf. Technol.* **2016**, *6*, 764. [[CrossRef](#)]
37. Yang, X.; Ren, H.; Wu, C.; Xiong, Y.; Ge, Q. Flexible Strain Sensors Fabricated by Fused Deposition Modeling-Based Multimaterial 3D Printing with Conductive Polyurethane Composites. In Proceedings of the 2021 27th International Conference on Mechatronics and Machine Vision in Practice (M2VIP), Shanghai, China, 26–28 November 2021; pp. 546–551.
38. Leigh, S.J.; Bradley, R.J.; Pursell, C.P.; Billson, D.R.; Hutchins, D.A. A Simple, Low-Cost Conductive Composite Material for 3D Printing of Electronic Sensors. *PLoS ONE* **2012**, *7*, e49365. [[CrossRef](#)]
39. Jain, A.; Prashanth, K.J.; Sharma, A.K.R.; Jain, A.; Rashmi, P.N. Dielectric and Piezoelectric Properties of PVDF/PZT Composites: A Review. *Polym. Eng. Sci.* **2015**, *55*, 1589–1616. [[CrossRef](#)]
40. Liu, K.; Hu, J.; Du, Y.; Shi, Y.; Sun, Y.; Zhang, S.; Tu, R.; Zhang, Q.; Huang, S.; Sun, H. Influence of Particle Size on 3D-printed Piezoelectric Ceramics via Digital Light Processing with Furnace Sintering. *Int. J. Appl. Ceram. Technol.* **2022**, *19*, 2461–2471. [[CrossRef](#)]
41. Renteria, A.; Fontes, H.; Diaz, J.A.; Regis, J.E.; Chavez, L.A.; Tseng, T.-L.; Liu, Y.; Lin, Y. Optimization of 3D Printing Parameters for BaTiO<sub>3</sub> Piezoelectric Ceramics through Design of Experiments. *Mater. Res. Express* **2019**, *6*, 085706. [[CrossRef](#)]
42. Mohammadi, M.; Coppola, B.; Montanaro, L.; Palmero, P. Digital Light Processing of High-Strength Hydroxyapatite Ceramics: Role of Particle Size and Printing Parameters on Microstructural Defects and Mechanical Properties. *J. Eur. Ceram. Soc.* **2023**, *43*, 2761–2772. [[CrossRef](#)]
43. Jaffe, H. Piezoelectric Ceramics. *J. Am. Ceram. Soc.* **1958**, *41*, 494–498. [[CrossRef](#)]
44. Isupov, V.A. Phases in the PZT Ceramics. *Ferroelectrics* **2002**, *266*, 91–102. [[CrossRef](#)]
45. Panda, P.K.; Sahoo, B. PZT to Lead Free Piezo Ceramics: A Review. *Ferroelectrics* **2015**, *474*, 128–143. [[CrossRef](#)]
46. Hu, X.; Li, X.; Yan, K.; Qi, X.; Chen, W.; Wu, D. Fabrication of Porous PZT Ceramics Using Micro-Stereolithography Technology. *Ceram. Int.* **2021**, *47*, 32376–32381. [[CrossRef](#)]
47. Hall, S.E.; Regis, J.E.; Renteria, A.; Chavez, L.A.; Delfin, L.; Vargas, S.; Haberman, M.R.; Espalin, D.; Wicker, R.; Lin, Y. Paste Extrusion 3D Printing and Characterization of Lead Zirconate Titanate Piezoelectric Ceramics. *Ceram. Int.* **2021**, *47*, 22042–22048. [[CrossRef](#)]
48. Smolenskii, G.A.; Agranovskaya, A.I. Dielectric Polarization and Losses of Some Complex Compounds. *Zhurnal Tekhnicheskoy Fiz.* **1958**, *28*.
49. Kuwata, J.; Uchino, K.; Nomura, S. Dielectric and Piezoelectric Properties of 0.91Pb(Zn<sub>1/3</sub>Nb<sub>2/3</sub>)O<sub>3</sub>-0.09PbTiO<sub>3</sub> Single Crystals. *Jpn. J. Appl. Phys.* **1982**, *21*, 1298. [[CrossRef](#)]
50. Li, F.; Zhang, S.; Xu, Z.; Wei, X.; Luo, J.; ShROUT, T.R. Composition and Phase Dependence of the Intrinsic and Extrinsic Piezoelectric Activity of Domain Engineered (1-x)Pb(Mg<sub>1/3</sub>Nb<sub>2/3</sub>)O<sub>3</sub>-xPbTiO<sub>3</sub> Crystals. *J. Appl. Phys.* **2010**, *108*, 034106. [[CrossRef](#)]
51. Roberts, S. Dielectric and Piezoelectric Properties of Barium Titanate. *Phys. Rev.* **1947**, *71*, 890–895. [[CrossRef](#)]
52. Ming, B.-Q.; Wang, J.-F.; Qi, P.; Zang, G.-Z. Piezoelectric Properties of (Li, Sb, Ta) Modified (Na,K)NbO<sub>3</sub> Lead-Free Ceramics. *J. Appl. Phys.* **2007**, *101*, 054103. [[CrossRef](#)]
53. Gao, D.; Kwok, K.W.; Lin, D.; Chan, H.L.W. Microstructure, Electrical Properties of CeO<sub>2</sub>-Doped (K 0.5 Na 0.5) NbO<sub>3</sub> Lead-Free Piezoelectric Ceramics. *J. Mater. Sci.* **2009**, *44*, 2466–2470. [[CrossRef](#)]
54. Lee, M.H.; Kim, D.J.; Park, J.S.; Kim, S.W.; Song, T.K.; Kim, M.-H.; Kim, W.-J.; Do, D.; Jeong, I.-K. High-Performance Lead-Free Piezoceramics with High Curie Temperatures. *Adv. Mater.* **2015**, *27*, 6976–6982. [[CrossRef](#)]
55. Woodward, D.I.; Pursell, C.P.; Billson, D.R.; Hutchins, D.A.; Leigh, S.J. Additively-Manufactured Piezoelectric Devices. *Phys. Status Solidi A* **2015**, *212*, 2107–2113. [[CrossRef](#)]
56. Jiang, Z.; Cheng, L.; Zeng, Y.; Zhang, Z.; Zhao, Y.; Dong, P.; Chen, J. 3D Printing of Porous Scaffolds BaTiO<sub>3</sub> Piezoelectric Ceramics and Regulation of Their Mechanical and Electrical Properties. *Ceram. Int.* **2022**, *48*, 6477–6487. [[CrossRef](#)]
57. Rabkin, B.A.; Zderic, V.; Vaezy, S. Hyperecho in Ultrasound Images of HIFU Therapy: Involvement of Cavitation. *Ultrasound Med. Biol.* **2005**, *31*, 947–956. [[CrossRef](#)]
58. Chen, Y.; Bao, X.; Wong, C.-M.; Cheng, J.; Wu, H.; Song, H.; Ji, X.; Wu, S. PZT Ceramics Fabricated Based on Stereolithography for an Ultrasound Transducer Array Application. *Ceram. Int.* **2018**, *44*, 22725–22730. [[CrossRef](#)]
59. Chen, Z.; Song, X.; Lei, L.; Chen, X.; Fei, C.; Chiu, C.T.; Qian, X.; Ma, T.; Yang, Y.; Shung, K.; et al. 3D Printing of Piezoelectric Element for Energy Focusing and Ultrasonic Sensing. *Nano Energy* **2016**, *27*, 78–86. [[CrossRef](#)]

60. Gaytan, S.M.; Cadena, M.A.; Karim, H.; Delfin, D.; Lin, Y.; Espalin, D.; MacDonald, E.; Wicker, R.B. Fabrication of Barium Titanate by Binder Jetting Additive Manufacturing Technology. *Ceram. Int.* **2015**, *41*, 6610–6619. [[CrossRef](#)]
61. Liu, K.; Zhou, C.; Hu, J.; Zhang, S.; Zhang, Q.; Sun, C.; Shi, Y.; Sun, H.; Yin, C.; Zhang, Y.; et al. Fabrication of Barium Titanate Ceramics via Digital Light Processing 3D Printing by Using High Refractive Index Monomer. *J. Eur. Ceram. Soc.* **2021**, *41*, 5909–5917. [[CrossRef](#)]
62. Cui, H.; Yao, D.; Hensleigh, R.; Lu, H.; Calderon, A.; Xu, Z.; Davaria, S.; Wang, Z.; Mercier, P.; Tarazaga, P. Design and Printing of Proprioceptive Three-Dimensional Architected Robotic Metamaterials. *Science* **2022**, *376*, 1287–1293. [[CrossRef](#)]
63. Omoniyi, O.A.; Mansour, R.; Reid, A.; Liang, L.; O’Leary, R.; Windmill, J.F.C. 3D-Printing of a Piezocomposite Material with High Filler Content for Transducer Applications. In Proceedings of the 2020 IEEE International Ultrasonics Symposium (IUS), Las Vegas, NV, USA, 7–11 September 2020; pp. 1–3.
64. Song, X.; Chen, Z.; Lei, L.; Shung, K.; Zhou, Q.; Chen, Y. Piezoelectric Component Fabrication Using Projection-Based Stereolithography of Barium Titanate Ceramic Suspensions. *Rapid Prototyp. J.* **2017**, *23*, 44–53. [[CrossRef](#)]
65. Sotov, A.; Kantyukov, A.; Popovich, A.; Sufiiarov, V. LCD-SLA 3D Printing of BaTiO<sub>3</sub> Piezoelectric Ceramics. *Ceram. Int.* **2021**, *47*, 30358–30366. [[CrossRef](#)]
66. Kim, H.; Renteria-Marquez, A.; Islam, M.D.; Chavez, L.A.; Garcia Rosales, C.A.; Ahsan, M.A.; Tseng, T.-L.B.; Love, N.D.; Lin, Y. Fabrication of Bulk Piezoelectric and Dielectric BaTiO<sub>3</sub> Ceramics Using Paste Extrusion 3D Printing Technique. *J. Am. Ceram. Soc.* **2019**, *102*, 3685–3694. [[CrossRef](#)]
67. Chen, W.; Wang, F.; Yan, K.; Zhang, Y.; Wu, D. Micro-Stereolithography of KNN-Based Lead-Free Piezoceramics. *Ceram. Int.* **2019**, *45*, 4880–4885. [[CrossRef](#)]
68. Mariani, M.; Beltrami, R.; Migliori, E.; Cangini, L.; Mercadelli, E.; Baldisserri, C.; Galassi, C.; Lecis, N. Additive Manufacturing of Lead-Free KNN by Binder Jetting. *J. Eur. Ceram. Soc.* **2022**, *42*, 5598–5605. [[CrossRef](#)]
69. Li, Y.; Li, L.; Li, B. Direct Ink Writing of Three-Dimensional (K, Na) NbO<sub>3</sub>-Based Piezoelectric Ceramics. *Materials* **2015**, *8*, 1729–1737. [[CrossRef](#)]

**Disclaimer/Publisher’s Note:** The statements, opinions and data contained in all publications are solely those of the individual author(s) and contributor(s) and not of MDPI and/or the editor(s). MDPI and/or the editor(s) disclaim responsibility for any injury to people or property resulting from any ideas, methods, instructions or products referred to in the content.